Macromolecules

Article

pubs.acs.org/Macromolecules

Modification of Melt-Spun Isotactic Polypropylene and Poly(lactic acid) Bicomponent Filaments with a Premade Block Copolymer

Sara A. Arvidson,[†] Kristen E. Roskov,[†] Jaimin J. Patel,[†] Richard J. Spontak,[†,‡] Saad A. Khan,*[,†] and Russell E. Gorga*[,§]

[†]Department of Chemical & Biomolecular Engineering, North Carolina State University, Raleigh, North Carolina 27695, United States

[‡]Department of Materials Science & Engineering, North Carolina State University, Raleigh, North Carolina 27695, United States

[§]Department of Textiles Engineering, Chemistry & Science, North Carolina State University, Raleigh, North Carolina 27695, United States

ABSTRACT: While numerous studies have investigated the effect of adding a block copolymer as a macromolecular surfactant to immiscible polymer blends, no such efforts have sought to alter the properties of melt-spun bicomponent core–sheath filaments with a nonreactive compatibilizing agent. In this study, we examine the effect of adding poly[styrene-*b*-(ethylene-*co*-butylene)-*b*-styrene] (SEBS) triblock copolymer to core–sheath filaments consisting of isotactic polypropylene (iPP) and poly(lactic acid) (PLA). Incorporation of the copolymer into blends of iPP/PLA is observed to reduce the size scale of phase separation. Interfacial slip between molten iPP and PLA layers is evaluated by rheology under steady-shear conditions. Addition of SEBS to the PLA sheath during filament formation reduces the tendency of PLA sheaths to crack prior to iPP core failure during tensile testing. In reversed filament configurations, the copolymer does not hinder the development of molecular orientation, related to fiber strength, during fiber spinning. Electron microscopy reveals that the copolymer molecules form unique, highly nonequilibrium morphologies under the spinning conditions employed here.

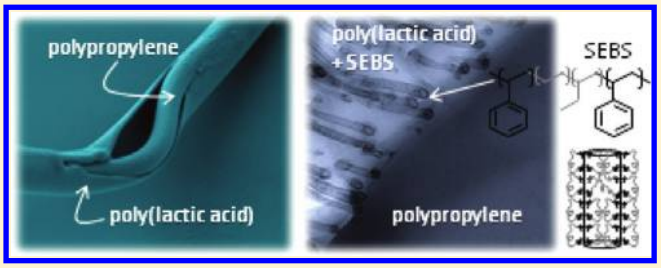

INTRODUCTION

Polymers produced from sustainable resources are expected to become increasingly important as petroleum feedstocks become less secure. Polylactide, or poly(lactic acid), (PLA) is produced from lactide monomer, which is obtained from agricultural rather than petroleum raw materials and is especially interesting because it is also biocompatible and biodegradable. Currently PLA is used in sutures, medical devices, and food packaging films.[1] It is a fiber-forming polymer with high tensile strength[2] but suffers from brittleness and low ductility,[3] poor gas barrier properties,[4] and hydrolysis at temperatures suitable for melt processing, dyeing, or laundering.[5−7] Cospinning PLA with a second polymer provides a route to overcome these challenges by producing bicomponent fiber with suitable mechanical properties.

Bicomponent filament spinning involves the coextrusion of two polymers (or polymer blends) from the same spinneret into a single filament that consists of both starting materials. This type of spinning can be configured in a variety of cross-sectional geometries such as core–sheath, side-by-side, segmented pie, islands-in-the sea, or tipped trilobal.[8−10] In this study, we only consider further the core–sheath arrangement. The benefits of cospinning two polymers include a reduction in the cost associated with using less of a more expensive polymer to obtain the same desirable characteristics or adding an expensive additive to only the sheath polymer, exploiting the lower melting point of a polymer spun in the sheath to promote bonding without a disruption in the morphology of the core component, improving the tactile quality of fabrics made from a spinnable polymer (sheath) with a polymer of poor spinnability (core), and suppression of an unfavorable rheological behavior (e.g., spinning a polymer behaving as a Newtonian liquid with a small fraction of a desirable polymer exhibiting Maxwell properties).[11] Moreover, since the viscoelasticity of the sheath polymer dictates the mechanics of melt flow during coaxial spinning even if its flow rate and viscosity are lower than those of the core polymer, core–sheath bicomponent fibers may be significantly thinner than would otherwise be achieved by spinning the polymers individually.[11] Lastly, while the bicomponent spinning of two polymers permits retention of component properties, comparable spinning of premixed polymer blends generally results in properties that lie intermediate between those of the individual components, thus compromising the net properties of the fibers.[12]

Isotactic polypropylene (iPP) constitutes an excellent choice for cospinning with PLA to impart improved mechanical properties; resistance to abrasion, solvents and biological agents (if iPP is the sheath component); and low cost. Furthermore,

Received: October 6, 2011
Revised: December 14, 2011
Published: January 3, 2012

iPP melts and can be processed at the same temperatures as PLA and can be viscosity-matched to PLA. Conversely, PLA provides a route to surface functionalize iPP, which is otherwise inert to many postspinning treatment processes available to other polymers, reduce fossil fuel consumption and greenhouse gas emission per mass of filament produced,[13] impart hydrophilicity, and direct the development of molecular orientation within iPP during fiber formation.[14]

Depending on the thermodynamic compatibility of the polymers involved, bicomponent spinning can result in filaments or fibers (used interchangeably throughout text) that fail by splitting when subjected to an external mechanical force.[15] While splittable fibers may be desired in the manufacture of synthetic suede and leather, technical wipes, and some filtration applications,[16−18] good adhesion between the individual species comprising bicomponent fibers is required for maintaining mechanical integrity, developing sutures, or improving chemical or flammability resistance.[19−22] At the interface separating immiscible polymers, a relatively low population of entanglements can lead to fiber delamination at temperatures below the melting temperatures (T_ms) of both components. Above the T_m of each component, subjecting immiscible polymers to external forces may result in "slip" of one molten polymer across the other. Evaluating the presence of slip and, by inference, the adequacy of interfacial chain entanglements in the melt remains a nontrivial task. Zhao and Macosko[23] have deduced that slip of multilayered samples occurs when a drop in viscosity accompanies an increase in the number of layers and, hence, interfacial contact area. Jiang[24] has similarly interpreted that a viscosity below the theoretical viscosity discerned from the reciprocal rule of mixtures (R-ROM) for layered high-density polyethylene/polystyrene (HDPE/PS) is indicative of slip. Slip has also been proposed as the cause for the viscosity discontinuity encountered while shearing layered HDPE/PS filled with tracer particles and observing the layers *in situ* with confocal microscopy.[25] Park et al.[26] have likewise investigated multilayer slip by using a sliding plate rheometer equipped with a camera.

Block copolymers, composed of two or more long, covalently linked sequences of chemically dissimilar repeat units, may be used to lower interfacial tension along polymer−polymer interfaces and thus improve adhesion by promoting chain entanglements. The apparent results of such compatibilization are net reductions in slip during extrusion and delamination in formed fibers.[27,28] Generally speaking, compatibilization is considered to be effective if an added block copolymer reduces the size scale of phase domains and/or enhances the mechanical properties of a blend.[12,29,30] The stabilizing efficacy and spatial segregation of premade block copolymer molecules along polymer−polymer interfaces have been previously addressed by Wei et al.[31] and more recently by Gozen et al.[32] Alternatively, reactive compatibilization of polymer blends can be induced through the use of species that react along the polymer−polymer interface to form block copolymers *in situ*.[33] In this spirit, blends of iPP and PLA have been modified with a maleic anhydride (MA)-grafted copolymer, which has been shown[34] to increase the impact strength of the resultant alloy. Similarly, iPP-*g*-MA has also been reported[35] to reactively cross-link core−sheath and side-by-side bicomponent fibers composed of nylon-6 and iPP. The concept of compatibilizing polymer−polymer interfaces that are not blended but rather contacted, such as those involved in core−sheath fibers or laminates, with premade block copolymers has largely been ignored. To the best of our knowledge, no prior studies investigating the core−sheath compatibilization of bicomponent fibers by the addition of a block copolymer to one component have been reported.

During large-scale mechanical deformation, melt-spun bicomponent fibers composed of iPP and PLA are observed to possess interfacial voids that extend up to millimeters in length along the fiber axis. These voids are attributed to inherently poor interfacial adhesion between iPP and PLA.[15] In this work, we endeavor to compatibilize and thus improve the mechanical properties of these two nonblended polymers by incorporating a triblock copolymer during melt spinning. In addition to filament property assessment, the morphology of the block copolymer in filaments is compared to that formed during melt mixing without extrusion to elucidate the effect of high-shear spinning on block copolymer structuration. Electron microscopy reveals that unique, nonequilibrium copolymer morphologies are generated during bicomponent filament spinning. We also discuss the application of steady-shear rheological methods to evaluate slip at layered iPP−PLA interfaces and the effect of adding the block copolymer.

EXPERIMENTAL SECTION

Materials and Specimen Preparation. The iPP and PLA were provided by Sunoco Chemicals (Pittsburgh, PA; CP360H) and NatureWorks (Minnetonka, MN; 6202D), respectively. A premixed compound containing a poly[styrene-*b*-(ethylene-*co*-butylene)-*b*-styrene] (SEBS) triblock copolymer with 18.6 wt % styrene (according to the manufacturer) and an overall molecular weight of 67 kDa (according to independent size exclusion chromatography) was supplied by Kraton Polymers (Houston, TX). While the identity of the compounding material is proprietary, it is midblock-selective, which indicates that it is more aliphatic than aromatic in nature. We do not, however, discount the possibility that the compounding species (hereafter referred to as the "midblock extender") may be partially unsaturated, unlike the EB midblock of the copolymer. Reagent-grade dichloromethane (DCM) was purchased from Mallinckrodt Chemicals (Phillipsburg, NJ) and used as received.

Single and bicomponent filaments were melt-spun at various aspirator pressures on the Partners' Pilot Spunbond line located in the Nonwovens Cooperative Research Center at North Carolina State University. All filaments examined here were spun with a total mass throughput of 0.4 g/(hole min) at a fiber composition of 50/50 (w/w) core/sheath. In select cases, 5 wt % of the PLA (2.5 wt % of the total mass) was replaced with the SEBS copolymer. In these instances, the PLA and copolymer were melt-compounded and coextruded. Confluence of the molten PLA (or PLA + SEBS) and iPP occurred in the spin pack. Below the spin pack, bicomponent filaments were directed through the quench zone to an attenuation zone, where the aspirator pressure controlled the air velocity around the fibers and effectively the fiber spinning velocity. Nonbonded fibers were collected immediately following extrusion so that the as-spun fiber morphology could be examined. Fiber diameters were used to calculate the "spinning velocity" (V) at the point where the fibers solidified according to

$$V = \frac{Q}{\rho A_c} \tag{1}$$

where Q is the mass flow rate of polymer per spinneret hole, ρ is the fiber mass density, and A_c is the cross-sectional area of the fiber. For comparison with the bicomponent fibers, corresponding polymer blends (50/50 wt % iPP/PLA; 50/47.5/2.5 wt % iPP/PLA/SEBS) were prepared using a Haake-Buchler HBI System 90 twin-screw melt mixer operated at 185 °C. iPP/PLA blends with and without SEBS were immersed in DCM for ∼100 h under constant agitation at ambient temperature to selectively dissolve the PLA for morphological evaluation.

Specimen Characterization. X-ray diffraction (XRD) studies were conducted on a Bruker D-5000 diffractometer (Madison, WI) equipped with a Highstar area detector and using Cu Kα radiation (λ = 0.1542 nm) at 40 kV and 30 mA. Resultant 2-dimensional XRD patterns were normalized with respect to an empty sample holder and analyzed with the Bruker General Area Detector Diffraction System (GADDS) software. Mechanical testing of fibers was conducted at ambient temperature on an Instron Model 5544 extensiometer (Norwood, MA) fitted with a 5 N load cell. Single filaments with a gauge length of 28.6 mm were strained at a constant crosshead speed of 25.4 mm/min. Data were analyzed with the Bluehill v.2 software package, and a constant volume cylinder was assumed to calculate true stress. Representative stress–strain curves were obtained for specimens prepared at different fiber configurations and pressures after at least 10 trials. Optical microscopy of bicomponent fibers was performed on a Mach–Zehnder type interference microscope by Aus Jena (Jena, Germany) with polarized light (λ = 546 nm), and digital images were collected on a CCD camera for birefringence analysis. Both scanning and transmission electron microscopies (SEM and TEM, respectively) were employed to explore the morphologies of the fibers and blends prepared here. After using DCM to dissolve the PLA from melt-processed iPP/PLA blends, the remaining iPP matrix was sputter-coated with ~10 nm of Au and subsequently analyzed by SEM performed in an environmental FEI XL-30 microscope operated under high vacuum at 5 kV. The average size and standard deviation of the pores introduced by extracting PLA were discerned by measuring the diameter of 100 pores using the ImageJ software suite.

For complementary TEM examination of the block copolymer morphology, fibers were conformally sputter-coated with 30 nm of Au (as a barrier layer to avoid fiber contamination), embedded in epoxy, and microtomed at ambient temperature on a Leica UltraCut 7 with a diamond knife. Resultant sections were stained for 7 min with the vapor of 0.5% RuO_4(aq), which is a selective stain for the phenyl groups on the S blocks of the SEBS copolymer. Cross-sectional TEM images were acquired on a field-emission Hitachi HF2000 microscope operated at an accelerating voltage of 200 kV. Average microdomain sizes and their corresponding standard deviations were determined by measuring 50–100 features of interest, unless otherwise noted, using ImageJ.

The zero-shear viscosities of the iPP and PLA homopolymers with and without copolymer, as well as multilayered samples thereof, were measured at 185 °C under nitrogen on a TA Instruments AR-G2 rheometer equipped with parallel plates measuring 25 or 40 mm in diameter. Multilayered specimens consisted of 1, 2, 4, or 8 alternating layers of iPP and PLA. Dynamic rheology was likewise performed on the same instrument operated at 185 °C with 25 mm plates and a 1 mm gap. Differential scanning calorimetry (DSC) was conducted on a TA Instruments Q2000 model calorimeter calibrated to an indium standard. Scans were carried out at heating rates of 10 °C/min under 50 mL/min N_2 purge with samples of ~10 mg in standard aluminum pans.

RESULTS AND DISCUSSION

Bicomponent iPP/PLA Fibers. Lipscomb[36] predicts that, for situations wherein the core polymer undergoes a greater increase in viscosity during cooling than the sheath polymer, the core polymer bears more of the spinline tension, which we hasten to add can serve to enhance crystallization and molecular orientation. Similarly, Kikutani[19] reports that the solidification temperature and viscosity disparities in cospun polymers constitute the main factors influencing the "mutual interactions" of the constituent polymers. This conclusion is interpreted to relate to the ability of one polymer to direct or influence the crystallization and molecular orientation of the other polymer. On one hand, we find that the crystallization of PLA is not strongly influenced by its location (i.e., core or sheath) in bicomponent fibers, as seen in Figure 1. (Representative XRD reflections for iPP/PLA bicomponent fibers are available in our previous work.[15]) The iPP crystal morphology, on the other hand, is sensitively affected by the fiber configuration. Our observation that iPP tends to crystallize in the sheath but not in the core, coupled with the results of Lipscomb[36] and our previous study[37] on the quiescent and stress-induced crystallization of iPP, suggests that iPP crystallization is due to exposure to the quench air while in the sheath and is not stress-induced while in the core. The presence of the iPP mesomorphic phase for most spinning velocities indicates an absence of high tension on the iPP core when cospun with a PLA sheath. (This may reflect the comparable melting temperatures and zero-shear viscosities of iPP and PLA, as listed in Table 1.) In marked contrast, Kikutani et al.[19] have demonstrated that cospinning iPP with poly(ethylene terephthalate) (PET) into bicomponent iPP_{sheath}/PET_{core} fibers results in sheaths that do not solidify in the draw zone and fibers that could not be drawn as finely as either constituent polymer. The difference in melting points between iPP and PET is significantly greater (~100 °C) than

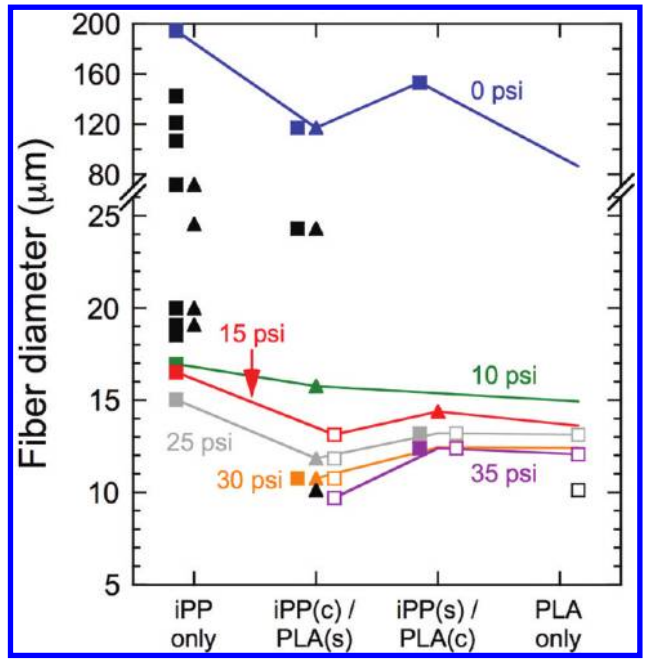

Figure 1. Filament diameter and polymer morphology as functions of aspirator pressure and fiber configuration, denoted by core (c) and sheath (s). While all filaments are at least partially amorphous, only crystalline or otherwise ordered morphologies are identified by symbols if present: α-crystalline iPP (filled squares), mesomorphic iPP (filled triangles), and α-crystalline PLA (open squares). Filaments spun at the same aspirator pressure with different configurations are connected by solid lines (color-coded and labeled).

Table 1. Physical Properties of the Polymers Employed in This Study

polymer	T_m[38] (°C)	zero-shear viscosity at 185 °C (Pa·s)	surface free energy[39] at 20 °C (dyn/cm)	solubility parameter[40,41] $(cal/cm^3)^{1/2}$
iPP	165[a]	901[a]	30.1	7.4
PLA	161[a]	591[a]	39.3	12.1
SEBS copolymer		6980[a]		
atactic polystyrene			40.7	9.5
low-density polyethylene			35.3	8.0
polybutylene			33.6	7.8

[a]Property was measured in the present study.

dx.doi.org/10.1021/ma202246h | Macromolecules 2012, 45, 913–925

that between iPP and PLA; this problem is not encountered here because the melt viscosities and thermal transitions of iPP and PLA are sufficiently similar so that neither polymer significantly influences the rheological properties or solidification behavior of the other compared to each polymer when spun individually.

According to the results displayed in Figure 1, an increase in aspirator pressure (and, correspondingly, spinning velocity) is generally accompanied by a reduction in fiber diameter that is significant from 0 to 10 psi for both single-component and bicomponent fibers. At a given aspirator pressure, the diameters of bicomponent fibers are often marginally lower than the fiber diameters of either polymer spun individually. This observation, along with the inherent thermodynamic incompatibility between iPP and PLA (discussed further in the next section), implies that the iPP/PLA interface may slip at high spin speeds, which occur at high shear rates. We return to address the occurrence of slip between molten iPP and PLA, as determined by rheology, later. Addition of the SEBS copolymer to PLA in bicomponent fibers is expected to influence the iPP/PLA interface and, by inference, the fiber morphology. Figure 2

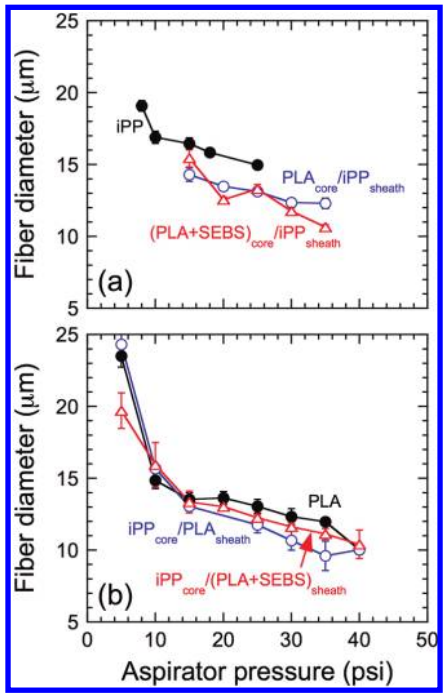

Figure 2. Filament diameter as a function of spinning pressure for different fiber configurations: (a) iPP only and iPP in the sheath (with PLA in the core) and (b) PLA only and PLA in the sheath (with iPP in the core). Homopolymers, bicomponent fibers without copolymer, and bicomponent filaments with copolymer are color-coded black, blue, and red and are correspondingly labeled. Error bars indicate the standard error in the data from ~10 trials, and the solid lines serve to connect the data.

shows the fiber diameters of bicomponent fibers cospun with and without copolymer. As is evident in Figures 1 and 2, an increase in aspirator pressure generally promotes a decrease in fiber diameter. Compared to iPP spun alone, finer fibers result from cospinning an iPP sheath around a PLA core (Figure 2a), but the addition of copolymer appears to have a nonsystematic effect on fiber diameter. With PLA as the sheath (Figure 2b), bicomponent fibers are slightly smaller in diameter at moderate spin speeds, and the addition of copolymer has little statistical effect on fiber diameter over the conditions examined.

Compatibilized iPP/PLA Blends. The interfacial energy between iPP and PLA is related to the surface energy of each polymer according to Antonoff's rule:

$$\gamma_{iPP-PLA} = |\gamma_{iPP} - \gamma_{PLA}| \quad (2)$$

From eq 2, the interfacial energy between iPP and PLA is estimated to be about 9 dyn/cm.[42,43] On the basis of the infinite-molecular-weight surface energies of the copolymer constituents (included in Table 1), addition of a SEBS block copolymer to an iPP/PLA blend lowers the interfacial tension at both the iPP−EB interface (3−5 dyn/cm) and the PS−PLA interface (~1 dyn/cm). Although Antonoff's rule is overly simplistic for many systems, it has been shown[44] to accurately describe the interfacial energy between PS and PLA. The interfacial energy provides a measure of thermodynamic incompatibility between two dissimilar species and contributes to the enthalpic portion of the system free energy. As such, it relates directly to the Flory−Huggins χ interaction parameter[45−47] and, by extension, to the corresponding difference in solubility parameters between the two species. The solubility parameters of all polymer species of interest here are also listed for comparison in Table 1. Solubility parameters are often used to estimate the compatibility of two polymers insofar as the species are relatively nonpolar and mixing is endothermic. While there is no general guideline for predicting polymer−polymer miscibility from solubility parameters alone,[39] polymer pairs with nearly identical solubility parameters are more likely to be mutually miscible than those with even modestly different solubility parameters, regardless of their chemical constitution.[48] On the basis of their solubility parameters, the EB midblock of the copolymer should be compatible with iPP, whereas the S endblocks of the copolymer are not expected to show much preference for either iPP or PLA. We cannot comment much on the compatibility of the midblock extender in the copolymer, but it stands to reason that, since it is mixed with the EB midblock, it, too, will be compatible with iPP.

To discern if the SEBS copolymer compatibilizes iPP/PLA blends, we examine the morphologies of blends composed of 50 wt % iPP. Figure 3a displays a cross-sectional SEM image of a melt-mixed iPP/PLA blend after removal of the dispersed PLA phase upon selective-solvent exposure in DCM at ambient temperature. The diameter of the PLA domains (appearing as pores) is measured to be 5.0 ± 2.9 μm. Replacing 5 wt % of the PLA with SEBS is found to reduce the PLA domain diameter to 1.4 ± 1.3 μm (cf. Figure 3b), which confirms that the copolymer effectively compatibilizes the iPP/PLA blends at this concentration, as anticipated from the thermodynamic considerations discussed above. It immediately follows that, if the copolymer molecules can locate along the interface between iPP and PLA, they should reduce slip (if it exists) during extrusion and improve the adhesion between iPP and PLA. Therefore, 2.5 wt % SEBS (5 wt % of the PLA phase) was also used for fiber-spinning experiments. It is of interest to note here that dissolution of the precompounded SEBS in DCM at a concentration of 5 wt % results in the formation of a cloudy solution that appears to remain stable to the unaided eye for several months at ambient temperature. We believe that the observed solution opacity arises from the self-organization of copolymer molecules into swollen micelles (spherical

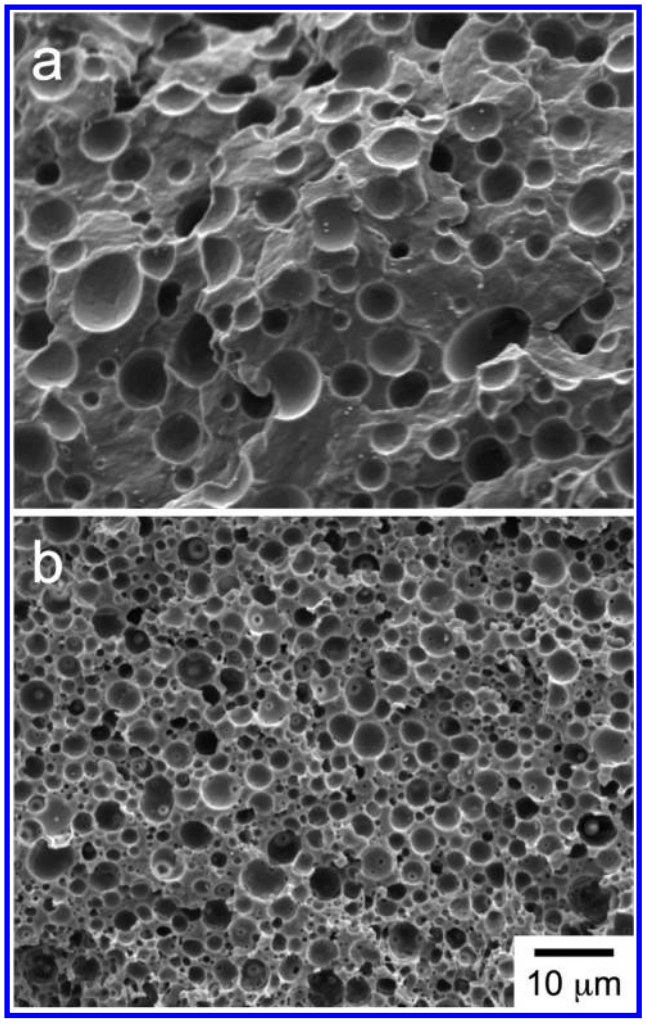

Figure 3. Cross-fracture SEM images of melt-mixed blends: (a) 50/50 w/w iPP/PLA and (b) 50/47.5/2.5 iPP/PLA/SEBS. The PLA is selectively removed upon immersion in DCM for ~100 h at ambient temperature.

microemulsions) or vesicles[49] that are sufficiently large to scatter light and encapsulate the midblock extender, which is most likely incompatible with DCM. A detailed account of this solution nanostructure is, however, beyond the scope of the present work.

Multilayer Melt Rheology. Various polymer pairs such as PS/poly(methyl methacrylate), PS/HDPE, PS/iPP, PE/fluoropolymer, and iPP/nylon-6 exhibit incompatibility-induced slip during rheological testing of layered specimens.[23,24,26] Layered specimens are more representative of the present bicomponent fibers than are blends because the two polymer species are melt-contacted along an artificially introduced interface rather than along multiple interfaces that develop *in situ* due to thermodynamic instability. Generally speaking, "slip", or negative viscosity deviation, tends to increase with increasing polymer−polymer incompatibility. To determine whether iPP and PLA undergo slip during extrusion, rheological testing has been conducted on alternating multilayers of iPP and PLA. As illustrated in Figure 4, these sandwich structures are first positioned on the bottom flat plate of the rheometer, and then the top plate of the rheometer is lowered until it contacts the top polymer layer. We have measured the shear viscosity of molten polymer multilayers as a function of

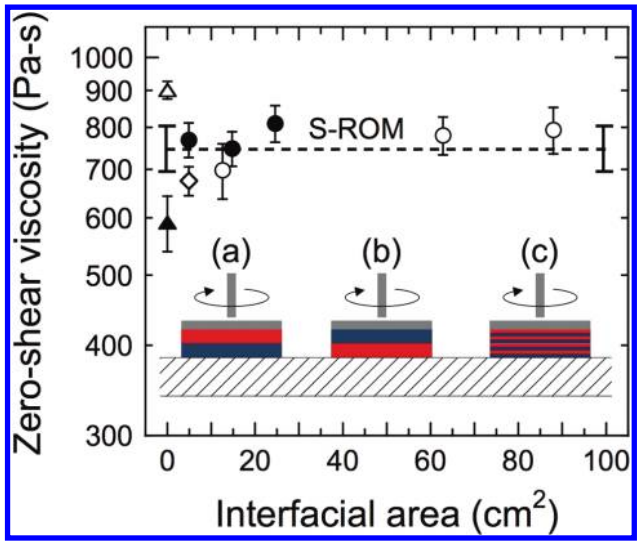

Figure 4. Zero-shear viscosities of iPP/PLA multilayers in different test configurations: PLA on the bottom with either 25 (●) or 40 (○) mm plates or iPP on the bottom with 25 mm plates (◇). Included are the individual viscosities of iPP (△) and PLA (▲). The error bars denote the standard error in the data, and the dashed line corresponds to the S-ROM prediction. The uncertainty of the prediction is based on the standard deviation of the neat iPP and PLA viscosities used to calculate the viscosity of the multilayers. Included are schematic illustrations of the iPP/PLA multilayers: (a) PLA (blue) on bottom, (b) iPP (red) on bottom, and (c) 8 alternating layers.

interfacial area, which is controllably manipulated by increasing the number of alternating layers, as well as the size of the plates. The zero-shear viscosities of these multilayers are presented as a function of interfacial area in Figure 4. To put these results into perspective, a melt-spun bicomponent fiber with an average inner diameter of 20 μm and measuring 1 m long would possess an interfacial area of ~0.6 cm^2. Despite the greater incompatibility between iPP and PLA as compared to other polymer pairs, no significant decrease in viscosity is detected with increasing interfacial area up to an interfacial area of ~90 cm^2, thereby indicating that slip between iPP and PLA is not detected by steady-shear rheology at stresses below ~1 kPa.

One reason for the absence of slip in this work may be due to the low shear rates accessible with a parallel-plate rheometer relative to capillary rheometers or fiber extrusion. Slip first becomes apparent, for instance, at interfacial areas between 34 and 152 cm^2 at shear stresses above 1 kPa for multilayers composed of iPP and PS.[23] Inertial forces cause the polymer to flow from the plates at stresses above 1 kPa, thereby resulting in poor data quality. Smaller parallel plates exacerbate this problem. Alternatively, we consider the manner by which previous studies concluded the existence of slip. While viscosities are reported,[23,24] the deviation from predicted "no-slip" conditions is often small. Because of the large variation in viscosity encountered in each sample, we have chosen to repeat each measurement seven times in this work. Jiang et al.[24] have reported the viscosity of a PS/HDPE bilayer with an interfacial area of about 5 cm^2 to be 11% lower than the reciprocal rule of mixtures (R-ROM). On the basis of this comparison, they conclude this deviation is representative of slip. To discern the validity of this criterion, we apply several rules of mixtures to the data in Figure 4. The first is the R-ROM, which has been used to predict the viscosity of multilayered specimens

composed of two polymers (indicated by subscripts 1 and 2). It is given by

$$\frac{1}{\eta} = \frac{\varphi_1}{\eta_1} + \frac{\varphi_2}{\eta_2} + \frac{\varphi_i}{\eta_i} \quad (3)$$

where the subscripted i corresponds to the interfacial layer, which has few polymer entanglements and potentially lower viscosity.[50] In eq 3, η is the measured viscosity of the multilayer, ϕ_1 and ϕ_2 are the volume fractions of polymers 1 and 2, respectively, and η_1 and η_2 are the viscosities of polymers 1 and 2, respectively, measured individually. Since no difference in viscosity is evident in Figure 4 up to an interfacial area of ~90 cm^2, this interfacial layer contribution is neglected.

Alternatively, other rules of mixtures should be considered. For example, the standard rule of mixtures (S-ROM) predicts viscosity according to

$$\eta = \varphi_1\eta_1 + \varphi_2\eta_2 \quad (4)$$

Moreover, a logarithmic rule of mixtures (L-ROM) has also been proposed for polymer blends, viz.[51]

$$\log \eta = \varphi_1 \log \eta_1 + \varphi_2 \log \eta_2 \quad (5)$$

Other rules include additional terms that attempt to explain deviations from the three provided in eqs 3−5 and are not considered here. The multilayer viscosity averaged over all the interfacial areas in Figure 4 is 754 Pa·s, whereas those predicted by eqs 3−5 are 714 (R-ROM), 746 (S-ROM), and 729 Pa·s (L-ROM). Thus, the S-ROM most closely predicts the viscosity of our multilayered samples, while the R-ROM is found to give the poorest prediction of the three. The standard errors of the PLA and iPP viscosities used in the ROM predictions are 9 and 3%, respectively, which suggests that measured multilayer viscosities deviating modestly (by 11% according to Jiang et al.[24]) from predicted values are not statistically significant in systems composed of iPP and PLA. The relatively large variation in measured multilayer and pure-component viscosities encountered here is indicative of the difficulty in confirming the existence of interfacial slip between iPP and PLA on a parallel-plate rheometer.

Fiber Mechanical Properties. The interface, which is largely responsible for the mechanical properties of bicomponent fibers (as well as fibers derived from polymer blends), is known[15] to fail during the mechanical drawing of bicomponent fibers spun from iPP and PLA. To reduce the inherent incompatibility between iPP and PLA, the SEBS copolymer is compounded with PLA before iPP and PLA are cospun. When PLA with and without copolymer is spun as the core (Figure 5a), the tenacity of the bicomponent fibers increases with increasing aspirator pressure up to a level near 2 cN/dtex. Incorporation of the copolymer has no systematic effect, positive or negative, on these results. Recall from Figure 1 that the PLA and iPP are both semicrystalline in this fiber configuration. If the fibers are spun with an iPP core and PLA sheath, a similar dependence on aspirator pressure is seen (Figure 5b), but the maximum level attained is slightly lower for fibers with PLA only and lower still (but within experimental uncertainty) for fibers with a mixture of PLA + SEBS. In this configuration, the PLA is semicrystalline, but the iPP is, for the most part, mesomorphic. Recall that, while the EB midblock of the SEBS copolymer is compatible with iPP, the S endblocks are not expected, on the basis of solubility parameters alone, to be strongly iPP- or PLA-compatible.

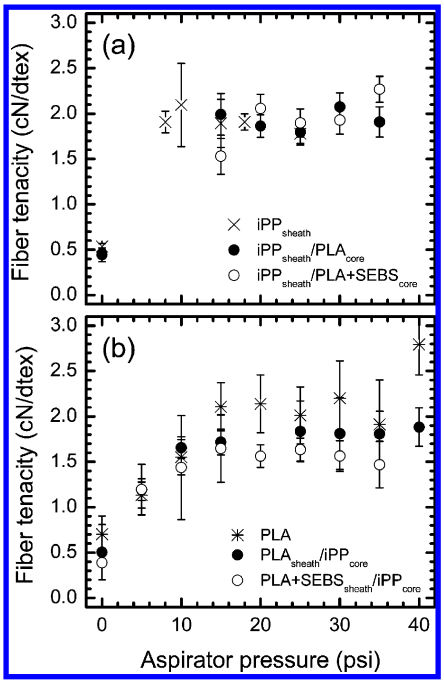

Figure 5. Dependence of tenacity of iPP, PLA, and bicomponent iPP/PLA filaments on aspirator pressure for two different fiber configurations identified by the location of the iPP: (a) sheath and (b) core. Open and filled symbols identify specimens with and without added SEBS copolymer, respectively. Error bars indicate the standard error in the data from ~10 trials.

Blending incompatible polymers into bicomponent fibers is expected to decrease fiber strength due to enlarged interfacial area and reduced interfacial strength. Yet, addition of the SEBS copolymer to PLA as the core (Figure 5a) or sheath (Figure 5b) does not compromise the mechanical properties of the fibers, indicating that the copolymer (with midblock extender) and PLA are not strongly incompatible.

At the lowest aspirator pressure (fiber spinning velocity) in Figure 6, addition of copolymer into the PLA sheath is

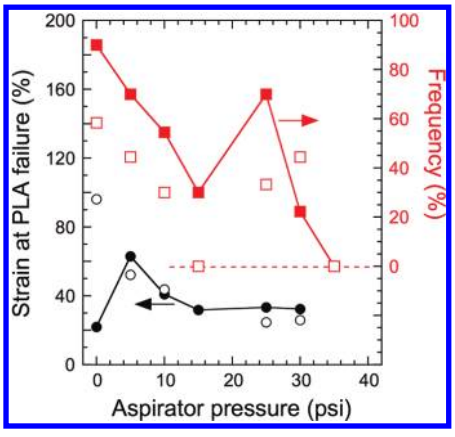

Figure 6. (left axis) True strain at which the sheath of iPP$_{core}$/PLA$_{sheath}$ bicomponent filaments with (○) and without (●) added SEBS copolymer fail as a function of aspirator pressure. (right axis, red) Frequency of PLA sheath failure prior to iPP core rupture with (□) and without (■) added copolymer. The solid lines serve to connect the data of systems without copolymer.

observed to increase substantially the strain at which rupture of the sheath occurs. As the aspirator pressure is increased,

dx.doi.org/10.1021/ma202246h | Macromolecules 2012, 45, 913−925

however, the strain at which PLA ruptures does not appear to be dependent on copolymer addition. Note that not all fibers undergo failure of the PLA sheath at lower strains than the iPP core. Rather, in these cases, a single catastrophic failure signals nearly simultaneous rupture of both polymers. Such events are accompanied by an abrupt increase in the true strain at break of the fibers. By adding the SEBS copolymer to PLA, the frequency at which the PLA sheath ruptures prior to failure of the iPP core is reduced at most aspirator pressures (cf. Figure 6), which indicates that the SEBS-modified PLA is capable of undergoing greater extension prior to failure. In the event that the PLA sheath does not fail before the iPP core (i.e., the sheath and core corupture) in any of the tested specimen, the frequency in Figure 6 is shown as 0%. While the T_g (Figure 7) and melt viscoelasticity (Figure 8) of PLA are not greatly

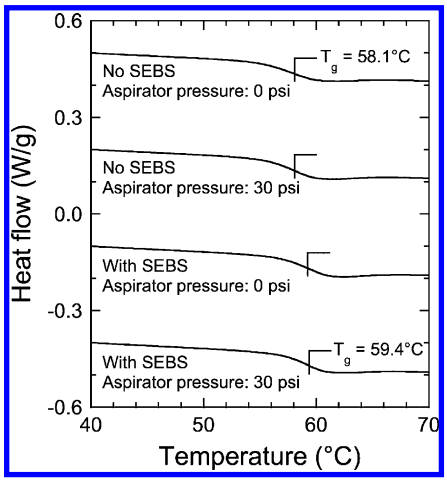

Figure 7. Series of DSC thermograms collected at a cooling rate of 10 °C/min from iPP_{core}/PLA_{sheath} bicomponent filaments with and without SEBS copolymer added to the PLA phase at two aspirator pressures (labeled). The location of the PLA T_g in each system is marked.

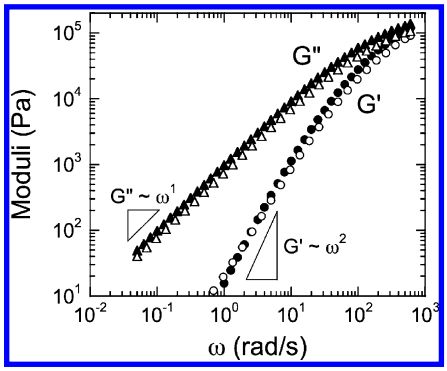

Figure 8. Frequency (ω) spectra of the dynamic moduli (G', circles; G'', triangles) measured from PLA (filled symbols) and PLA blended with 5 wt % SEBS (open symbols) at 185 °C and a stress of 5 Pa (in the linear viscoelastic limit). Shown for comparison are the scaling relationships expected for G' and G'' in the low-ω (terminal) region for entangled homopolymers.

affected by the incorporation of SEBS, the elastomeric nature of the copolymer, coupled with its intrinsic ability to self-organize into nanostructural elements, may serve to improve the elasticity of the PLA sheath, which, in turn, promotes an increase in the strain at which the PLA sheath ruptures. In Figure 7, addition of the SEBS copolymer alters the T_g of PLA by just over 1 °C, which is considered to be within instrumental uncertainty. The melt frequency (ω) spectra displayed in Figure 8 show little variation upon addition of the SEBS copolymer to PLA. In both cases, the dynamic loss modulus (G'') scales as $\omega^{1.0}$ in the terminal region, which agrees with the behavior of entangled homopolymers (ω^1). The analogous scaling behavior of the dynamic storage modulus (G'), which is ω^2 for entangled homopolymers, changes upon copolymer addition from $\omega^{1.9}$ to $\omega^{1.6}$. While this subtle reduction in slope may signify a copolymer-induced change in the molten structure, it is reasonable to expect that such a change might be more apparent in the solid state (where the styrenic endblocks are glassy) than in the melt. The copolymer-induced reduction in the frequency of PLA rupture at low strains may also indicate improved adhesion along the iPP/PLA interface, which would promote greater stress transfer to the iPP core and permit the PLA to support a higher stress before rupturing.

Previously, some of us have introduced[15] a facile optical method for estimating the molecular orientation of bicomponent core/sheath fibers from true stress–true strain curves when the refractive indices of the core and sheath polymers significantly differ. Figure 9 shows the progression of matching

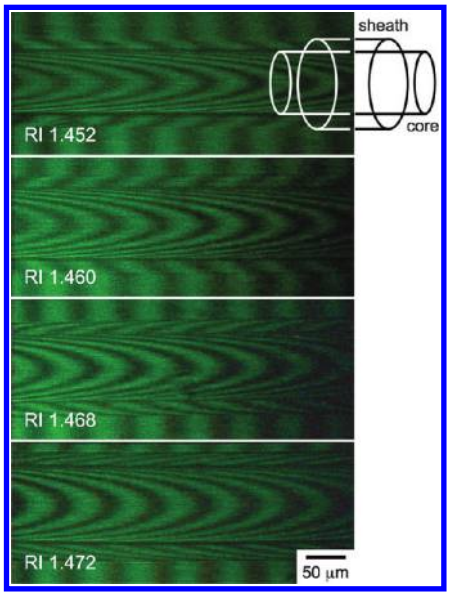

Figure 9. Optical micrographs of iPP_{core}/PLA_{sheath} bicomponent filaments (see schematic diagram) digitally recorded under polarized light to measure the birefringence according to ref 52. The measured birefringence can be related to molecular orientation and, thus, mechanical properties, as described elsewhere.[53,54] The refractive index (RI) provided on each image corresponds to that of the liquid surrounding the filament.

a fiber with an iPP core and PLA sheath to liquids of known refractive index so that the birefringence of the sheath, which is related to molecular orientation and fiber strength, can be determined. These images confirm that the conformal PLA sheath completely wets the iPP core. The liquid surrounding the fiber must possess a refractive index (RI) that is similar to those of the two species in the fiber to yield clear fringes (dark bands) that can be followed through each interface. Because the refractive indices of the iPP core and PLA sheath are considerably different (1.504 and 1.542, respectively, at 20 °C

dx.doi.org/10.1021/ma202246h | Macromolecules 2012, 45, 913–925

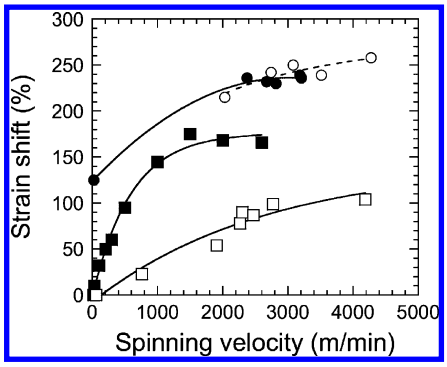

Figure 10. Dependence of the strain shift of iPP (■), PLA (□), PLA_{core}/iPP_{sheath} (●), and PLA + $SEBS_{core}/iPP_{sheath}$ (○) filaments on spinning velocity. The lines serve as guides for the eye.

for unoriented samples), no single liquid can provide clear fringes for both the core and sheath simultaneously, which explains why the fringes blur at the core−sheath and/or sheath−liquid interface in each of the images in Figure 9. In addition, while the interface of unstrained fibers appears continuous for the fibers in this study, birefringence measurements would be difficult or altogether impossible for strained iPP_{core}/PLA_{sheath} fibers exhibiting voids at the polymer−polymer interface. Therefore, using the method described elsewhere,[15] we estimate the molecular orientation of PLA_{core}/iPP_{sheath} fibers with and without added SEBS copolymer using stress−strain curves.

The strain shift of single-component and bicomponent fibers, which relates proportionally to molecular orientation, is presented as a function of spinning velocity in Figure 10. Here, spinning velocity, rather than aspirator pressure, is used to

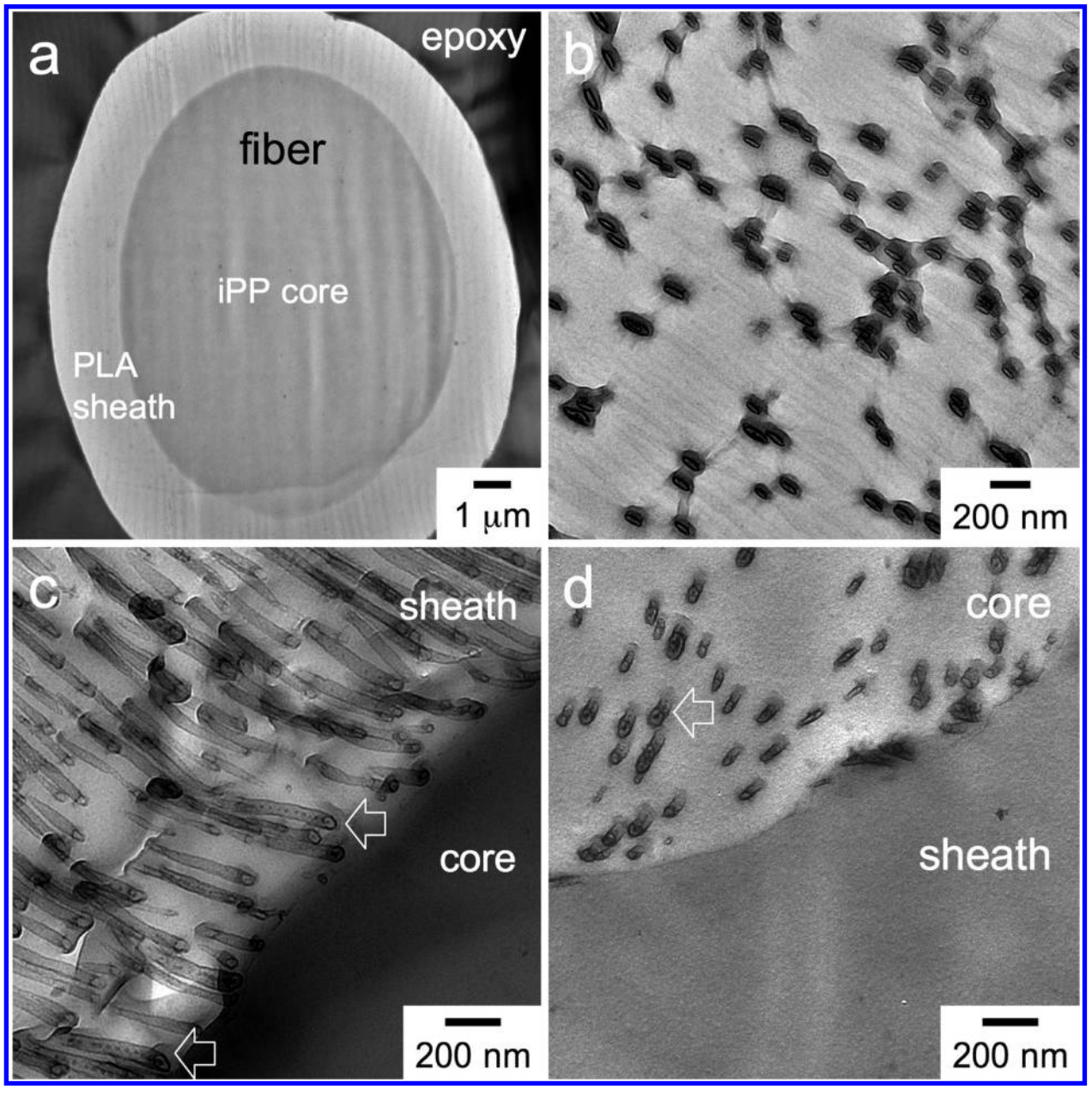

Figure 11. Cross-sectional TEM images of filaments in different configurations. In (a), an iPP_{core}/PLA_{sheath} bicomponent filament coated in Au and embedded in epoxy (labeled) is shown. A PLA filament modified with 5 wt % SEBS copolymer is presented in (b). In (c) and (d), $iPP_{core}/(PLA + SEBS)_{sheath}$ and $(PLA + SEBS)_{core}/iPP_{sheath}$ bicomponent filaments are displayed. The styrene-rich copolymer nanostructures appear dark due to selective staining. In (c) and (d), the arrowheads identify a unique nanostructure: tubules with internal spheres ("peas in a pod").

facilitate comparison of birefringence from fibers produced by other spinning methods, such as melt spinning or electrospinning, that do not require an aspirator pressure. Bicomponent fibers exhibit markedly increased strain shift relative to iPP and PLA alone, and addition of the SEBS copolymer to the PLA core does not inhibit molecular orientation in the iPP sheath. This observation is consistent with previous studies[11,15] reporting that the sheath component dictates flow mechanics for core/sheath fiber extrusion, as well as the ultimate properties of bicomponent fibers, since the sheath component experiences the greatest stress in both the melt and solid phases. Spinning with an iPP sheath and a PLA (or PLA + SEBS) core serves to focus the spin-line stress over a smaller cross-sectional area, which results in higher molecular orientation in the iPP sheath. While the sheath component may control flow mechanics, the core polymer is crucial to achieve the synergistic effect of enhanced molecular orientation in the sheath polymer beyond that realized by spinning either polymer individually. The master stress−strain curve for PLA required in this methodology has been developed for PLA alone, not with SEBS copolymer. Therefore, we do not report strain shifts for iPP_{core}/PLA_{sheath} fibers with and without SEBS to avoid attributing effects introduced by SEBS to changes in PLA molecular orientation.

Nonequilibrium Copolymer Morphologies. The morphologies of triblock copolymers, such as the SEBS copolymer employed in this study, have been the subject of numerous studies. Most commercial triblock copolymers are designed as thermoplastic elastomers with dispersed glassy microdomains embedded in, and connected to, a continuous, rubbery matrix.[55] Addition of a midblock-selective oil,[56] tackifying resin,[57] or homopolymer[58] to a triblock copolymer can yield the same morphologies observed in diblock copolymer/homopolymer blends,[59,60] in which case comparable design rules can be sensibly presumed. It immediately follows that, on the basis of the copolymer composition, the proprietary midblock extender added to the copolymer used here promotes a spherical or cylindrical morphology if the extender is largely or marginally miscible, respectively, with the EB midblock. Incorporation of the copolymer into PLA adds another level of complication, as the copolymer must now partition between the midblock extender and PLA as well as interact with iPP along the iPP−PLA interface. Under ideal equilibrium conditions of slow solvent evaporation or melt mixing, followed by extensive solvent or thermal annealing, the resultant copolymer morphology may be complex, depending on the individual strengths of six different binary interactions (assuming that the EB midblock and midblock extender can each be treated as a single species). If the rapid melt processing of the bicomponent fibers modified by the copolymer is now considered, highly nonequilibrium morphologies can be reasonably expected.

We begin with an overview of the morphologies of the SEBS copolymer in different fibers. Figure 11 shows a series of TEM images acquired from fibers varying in configuration, but spun at the same aspirator pressure (15 psi). In Figure 11a, a relatively low-magnification image of a bicomponent fiber composed of an iPP core and PLA sheath demonstrates that (i) the conformal Au coating around the edge of the fiber prevents swelling of the fiber with epoxy resin, which reacts with the vapor of RuO_4(aq), (ii) the iPP−PLA interface is clearly differentiated in cross section, and (iii) the iPP core is lightly stained. An image of a PLA fiber containing 5 wt % SEBS copolymer is provided in Figure 11b and reveals that the

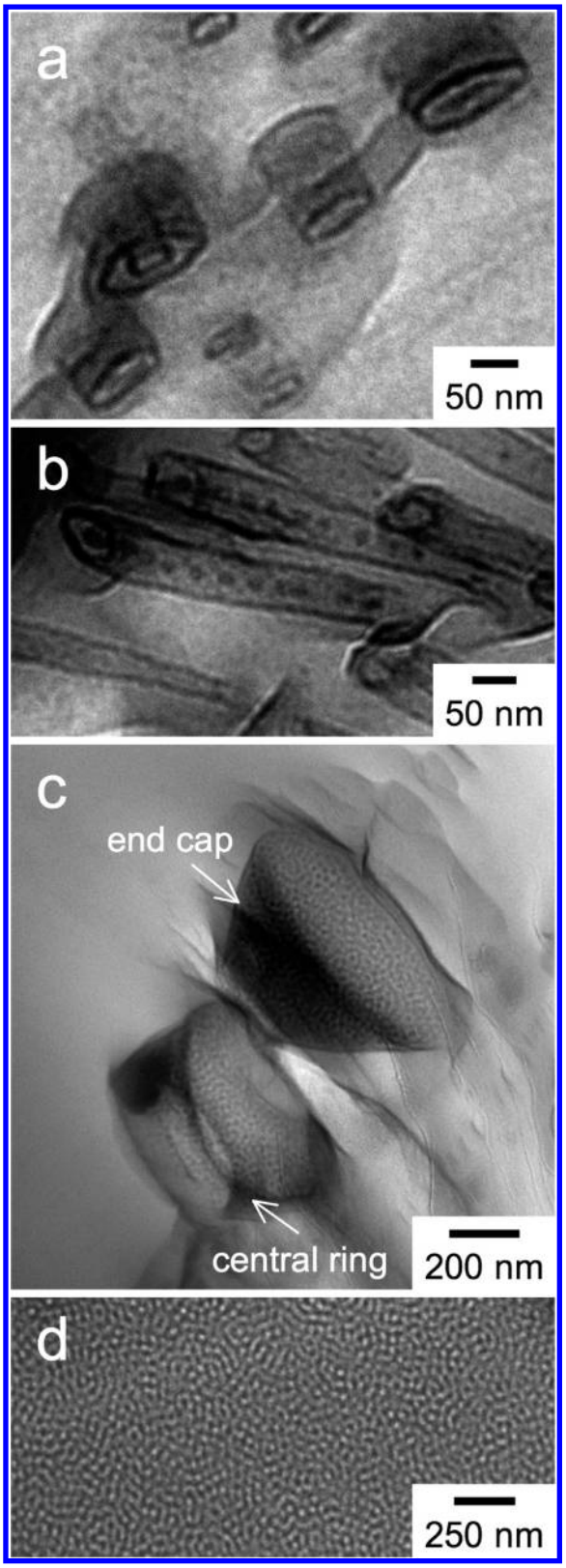

Figure 12. Series of TEM images showing unexpected morphologies of the SEBS copolymer after being compounded with PLA and melt-spun into bicomponent filaments. In (a), single tubules and concentric tubules are evident, whereas the "peas in a pod" morphology is clearly seen in (b). Large-scale structures that appear vesicular with ordered copolymer walls are visible in PLA melt-compounded with the SEBS copolymer prior to cospinning (c). The morphology of the as-received copolymer with midblock extender is provided for reference in (d).

dx.doi.org/10.1021/ma202246h | *Macromolecules* 2012, 45, 913−925

copolymer molecules, selectively stained with the vapor of RuO_4(aq), are present in the form of discrete and aperiodic nanostructures that most closely resemble dispersed tubules. The existence of tubules suggests that the midblock extender is either not highly compatible with the EB midblock of the copolymer or present at sufficiently high concentration to preclude appreciable solubilization within the copolymer matrix. Moreover, assuming that the copolymer is uniformly dispersed in the PLA prior to melt spinning, the styrenic endblocks of the copolymer do not appear to be very compatible with PLA.

In the TEM images displayed in Figures 11c and 11d, the copolymer morphologies formed in bicomponent iPP_{core}/$(PLA + SEBS)_{sheath}$ and $(PLA + SEBS)_{core}$/iPP_{sheath} fibers are evident. In both cases, copolymer molecules generate dispersed nanostructures that remain distributed throughout PLA rather than accumulating along the iPP−PLA interface. This tendency is consistent with the property measurements provided earlier and explains why the copolymer does not significantly alter the breaking strength of the bicomponent fibers investigated here. Although thermodynamic considerations indicate that the copolymer should migrate to the iPP−PLA interface, the time scale associated with fiber spinning is on par with or faster than that required for the diffusion of individual copolymer molecules from the PLA phase to the interface. To complicate matters further, the copolymer molecules are assembled into nanostructures that are less driven (due to a concentration gradient) and slower to diffuse to the interface where they are needed to compatibilize the core and sheath. Careful examination of the nanostructures observed in Figures 11c and 11d reveals that the copolymer nanostructures tend to orient along a common direction (which may be normal to the iPP−PLA interface) and, more importantly, that the copolymer molecules appear to self-organize into tubules, not cylinders, in PLA cospun with iPP. [Stained cylinders appear the most electron dense (darkest) along their centerline, whereas tubules are darkest along their periphery due to thickness considerations in projection.] While bicomponent block copolymers have been previously reported[61,62] to form nanotubes, such morphologies normally require an additional driving force, such as crystallization, to do so. The orientation of the tubules relative to the fiber axis could not be unequivocally determined from TEM images because TEM provides a 2D representation of a 3D object, wherein the orthogonal direction cannot be accurately determined. However, a series of images collected at different tilt angles have been carefully aligned as a precursor to transmission electron microtomography to qualitatively understand the relative orientation of the tubules with respect to neighboring tubules.

While it is intriguing that in all the core/sheath fiber configurations examined the copolymer molecules most often form tubules within PLA, more exotic morphologies, such as concentric tubules and spheres in tubules (what we term "peas in a pod"), are also observed, as evidenced by the TEM images provided in Figures 12a and 12b, respectively. Examples of the "peas in a pod" morphology are also highlighted in Figures 11c and 11d. A qualitatively similar sphere-in-cylinder morphology has been observed[63] in a thin film of an ABC triblock copolymer swollen with a good, neutral solvent. To the best of our knowledge, however, this morphology has not been previously reported for a blend of an ABA triblock copolymer dispersed in a C homopolymer. These highly nonclassical morphologies are schematically depicted in Table 2, and relevant dimensions identified in the illustrations and measured from TEM images are included. To put these dimensions into perspective, the unperturbed gyration diameter of the blocks comprising the SEBS copolymer are calculated from the freely jointed chain model[64] and the known block lengths. Since the EB midblock most likely adopts a looped or bridged conformation (which is rigorously true only at equilibrium), its molecular weight is halved so that it can be treated as a tail, a chain tethered at only one end, in similar fashion as the S endblocks. Block gyration diameters, estimated with the assumptions that (i) the statistical segment lengths of S and EB are comparable (~0.7 nm)[65,66] and (ii) the EB midblock consists of equal fractions of E and B, are ~4 nm for the S block and ~15 nm for (half) the EB block. The number of unperturbed blocks (N) corresponding to the measured dimensions identified in the diagrams shown in Table 2 is included in the same table and reveals several important features.

Analysis of the tubule walls generally yields $N \approx 2$, which corresponds to an endblock bilayer. This finding is consistent with the EB midblocks extending into both the tubular core and the surrounding matrix. In the case of a single tubule (morphology A in Table 2), the measured internal diameter also results

Table 2. Dimensions (in nm) of the SEBS Copolymer Morphologies Observed in Melt-Spun Bicomponent Fibers

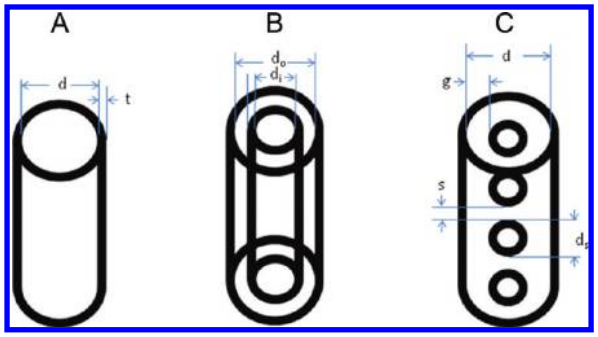

	morphology A		morphology B		morphology C			
core/sheath fiber configuration[a]	d (n)	t (n)	d_i (n)	d_0 (n)	d (n)	d_s (n)	s (n)	g (n)
PLA + SEBS in core	51 ± 31 (50)	8 ± 4 (50)	126 (1)	225 (1)	56 ± 16 (12)	16 ± 6 (32)	10 ± 4 (32)	17 ± 4 (32)
PLA + SEBS in sheath	30 ± 10 (50)	8 ± 2 (50)	70 (2)	100 (2)	42 ± 15 (13)	14 ± 4 (56)	13 ± 4 (56)	16 ± 5 (56)

[a] n denotes the number of features measured.

dx.doi.org/10.1021/ma202246h | Macromolecules 2012, 45, 913−925

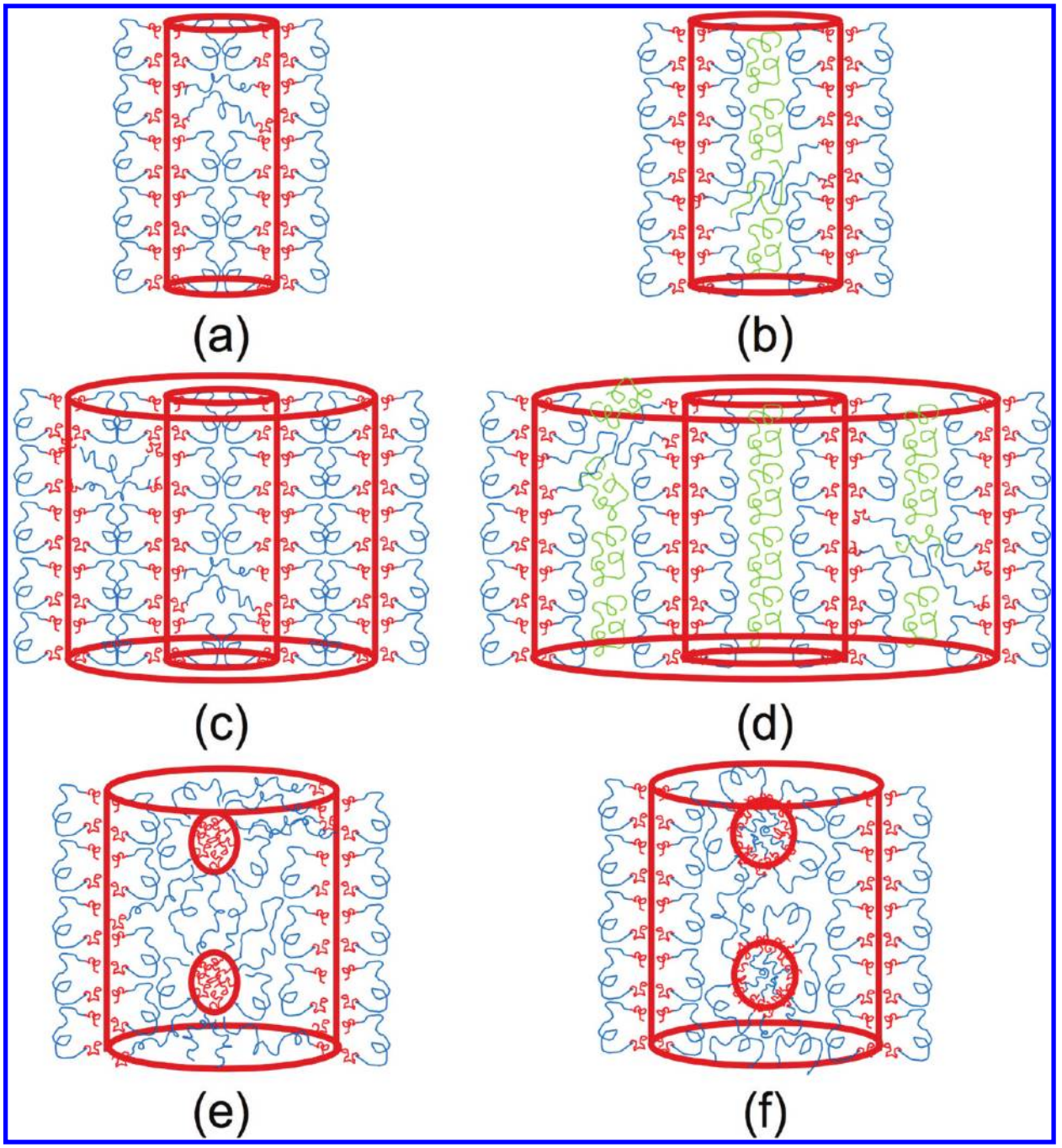

Figure 13. Schematic illustrations of the unexpected SEBS morphologies observed in melt-spun bicomponent filaments composed of iPP and PLA: (a) single tubules with bilayered S (red) walls, (b) tubules swollen with either the midblock extender or entrapped PLA (green), (c) concentric tubules that are connected by bridged EB midblocks (blue), (d) concentric tubules swollen with either the midblock extender or entrapped PLA, (e) equally sized and spaced S spheres in a single tubule ("peas in a pod"), and (f) equally sized and spaced core-shell S spheres in a single tubule.

in $N \approx 2$ (i.e., 2 EB blocks) for tubules formed in the (PLA + SEBS)$_{sheath}$ configuration but varies considerably from about 1 to 3 in the (PLA + SEBS)$_{core}$ configuration. This variation may reflect differences in the level of spin-line stress experienced by the copolymer molecules, as well as stochastic swelling of the EB midblock by the midblock extender or PLA. Similar variation is evident in the EB-rich regions of the concentric tubule morphology (morphology B in Table 2). Within the PLA + SEBS core, a single internal tubule appears highly swollen with $N \approx 8$, but the distance between the internal and external walls yields $N \approx 1$, which implies that the EB midblocks extending from the internal and external tubule walls are interdigitated into a monolayer, rather than bilayered. Lastly, in the "peas in a pod" morphology (morphology C in Table 2), the diameter of the internal spheres (which appear circular but, in a few cases, as shells) is significantly larger than two S endblocks ($N \approx 4$). These enlarged spheres are presumed to be the result of partial PLA incorporation, although the possibility of other kinetically trapped species cannot be outright disregarded. The distances between neighboring spheres (which align along the direction of the tubule) and between the spheres and tubule wall in both the core and sheath fiber configurations yields $N \approx 1$, which strongly suggests that the spheres are most likely connected

dx.doi.org/10.1021/ma202246h | *Macromolecules* 2012, 45, 913–925

together, as well as to the tubule walls, by bridged EB midblocks, as schematically depicted in Figure 13. Such molecular connectivity within the nanostructures present might serve to reinforce the PLA phase and improve its elasticity, as deduced from the flow and mechanical properties discussed earlier. It is comforting that these unique morphologies, although nonequilibrium in nature, tend to obey classical chain packing behavior.

In addition to establishing the presence of uncommon copolymer morphologies in bicomponent fibers, the images presented in Figures 11b, 11c, 12a, and 12b confirm that the S endblocks are not in direct contact with PLA. Rather, the EB midblock forms a contiguous coronal layer around the S-rich features. Such isolation helps to explain why the copolymer does not preferentially migrate to and accumulate along the iPP−PLA interface where it can promote compatibilization. To discern the extent to which the SEBS copolymer is dispersed within PLA prior to melt spinning, we have examined the melt-compounded PLA + SEBS mixture. Large structures such as those portrayed in Figure 12c are evident, indicating that the two materials are not thoroughly mixed. These macrostructures, measuring on the order of hundreds of nanometers across, also appear tubular (the figure displays a central "ring" and what appears to be an end-cap). Close examination of their walls reveals an organized copolymer nanostructure. Complementary inspection of the as-received copolymer with midblock extender (Figure 12d) confirms the existence of an irregular morphology that resembles the nanostructured walls of the macroscale tubules in Figure 12c. Thus, we conclude that the copolymer retains some of its as-received nanostructure after being melt-blended with PLA, indicating that the compounding temperature and mechanical mixing employed here were insufficient to molecularly disperse the copolymer within PLA.

On a side note, it is strangely curious, though, that the stainable, but minor, styrenic component in the as-received compound with the midblock extender appears as the matrix in Figure 12d, which suggests that the morphology may be more complicated than styrenic spheres or cylinders as previously anticipated. Although this figure is representative of entire sections of the as-received copolymer, it is likewise possible that the as-received copolymer is heterogeneous at macroscopic length scales. Such macroscale heterogeneity may be largely responsible for the unique nanoscale tubular morphologies reported here in Figures 11 and 12, as they could be the result of subjecting the parent morphologies in the heterogeneous PLA + SEBS mixture to very high shear and extensional flow through the spinneret during which time they became distorted and rearranged into lower-energy nanostructural elements. This nonequilibrium formation mechanism seems more plausible than conventional self-organization of the copolymer from a disordered state and would help to explain the variety of nanostructures observed on the basis of local copolymer composition and diffusion considerations.

■ CONCLUSIONS

The strategy of copolymer-induced blend compatibilization has been applied to melt-spun bicomponent fibers that bring together iPP and PLA in contact along a single interface separating the core from the sheath. Although the two polymers are incompatible, there is no evidence of measurable slip at the molten iPP−PLA interface according to steady-shear rheology. While the addition of a SEBS copolymer to a melt-mixed iPP/PLA blend serves as a compatibilizer by reducing the size of PLA domains arising from macrophase separation, incorporation of the copolymer into PLA prior to cospinning does not drastically improve the properties of bicomponent iPP/PLA fibers, which implies that the copolymer molecules are unable to concentrate along the iPP−PLA interface during spinning. Despite an absence of copolymer along the fiber interface, the strain at which PLA as the sheath ruptures increases sharply at low spinning pressure, and the number of fibers that undergo failure of the PLA sheath prior to failure of the iPP core is reduced by up to 30%, upon addition of copolymer. Thus, although the copolymer does not modify the iPP−PLA interface, it does affect the host PLA by improving its elasticity through the formation of unique copolymer nanostructures that include single tubular, concentric tubular, and "peas in a pod" morphologies. Careful analysis of such unexpected morphologies confirms the existence of nanostructural dimensions capable of accommodating local connectivity through midblock bridging, which consequently allows these highly elastic, EB-rich copolymer dispersions to rubber-toughen[67] the PLA.

■ ACKNOWLEDGMENTS

Financial support of this work has been provided by the Nonwovens Cooperative Research Center at North Carolina State University and the National Science Foundation through a Graduate Research Fellowship (K.E.R.). We thank Dr. Behnam Pourdeyhimi for insightful and fruitful discussions, as well as Christina Tang and Alina Higham for analytical assistance.

■ REFERENCES

(1) Mutsuga, M.; Kawamura, Y.; Tanamoto, K. *Food Addit. Contam., Part A* **2008**, *25* (10), 1283−1290.
(2) Mezghani, K.; Spruiell, J. *J. Appl. Polym. Sci.* **1998**, *36*, 1005−1012.
(3) Murariu, M.; Ferreira, A. D.; Alexandre, M.; Dubois, P. *Polym. Adv. Technol.* **2008**, *19* (6), 636−646.
(4) Nyambo, C.; Mohanty, A. K.; Manjusri, M. *Biomacromolecules* **2010**, *11* (6), 1654−1660.
(5) Agarwal, M.; Koelling, K. W.; Chalmers, J. J. *Biotechnol. Prog.* **1998**, *14* (3), 517−526.
(6) Holm, V. K.; Ndoni, S.; Risbo, J. *J. Food Sci.* **2006**, *71* (2), E40−E44.
(7) Mohd-Adnan, A. F.; Nishida, H.; Shirai, Y. *Polym. Degrad. Stab.* **2008**, *93* (6), 1053−1058.
(8) Kabeel, M. A. *Rev. Sci. Instrum.* **1991**, *62*, 2950−2954.
(9) Sun, C.; Zhang, D.; Liu, Y.; Xiao, J. *J. Ind. Text.* **2004**, *34*, 17−26.
(10) Fedorova, N.; Pourdeyhimi, B. *J. Appl. Polym. Sci.* **2007**, *104*, 3434−3442.
(11) Park, C.-W. *AIChE J.* **1990**, *36* (2), 197−206.
(12) Holsti-Miettinen, R.; Seppälä, J.; Ikkala, O. T. *Polym. Eng. Sci.* **1992**, *32*, 868−877.
(13) Cargill, Inc. http://www.cargill.com/corporate-responsibility/environmental-innovation/pioneering-new-business/corn-plastic/index.jsp (accessed 06/30/2010). Kimura, K. *Fujitsu Sci. Tech. J.* **2005**, *41* (2), 173−180.
(14) Fuentes, C. A.; Tran, L. Q. N.; Dupont-Gillain, C.; Vanderlinden, W.; De Feyter, S.; Van Vuurea, A. W.; Verpoest, I. *Colloids Surf., A* **2011**, *380*, 89−99.
(15) Arvidson, S. A.; Wong, K. C.; Gorga, R. E.; Khan, S. A. *Polymer* (in revision).
(16) Okamoto, M.; Mizuguchi, S.; Watanabe, K. U.S. Patent #3,705,226, Dec 5, 1972.
(17) Dugan, J. *Critical factors in engineering segmented bicomponent fiber for specific end uses*, 1999 (http://www.FITfibers.com/Publications.htm).
(18) Fruedenburg and Co kg. (http://www.evolon.com).

(19) Kikutani, T.; Radhakrishnan, J.; Arikawa, S.; Takaku, A.; Okui, N.; Jin, X.; Niwa, F.; Kudo, Y. *J. Appl. Polym. Sci.* **1996**, *62*, 1913−1924.
(20) Cho, H. H.; Kim, K. H.; Kang, Y. A.; Ito, H.; Kikutani, T. *J. Appl. Polym. Sci.* **2000**, *77*, 2254−2266.
(21) Houis, S.; Schmid, M.; Lubben, J. *J. Appl. Polym. Sci.* **2007**, *106*, 1757−1767.
(22) Im, J. N.; Kim, J. K.; Kim, H. K.; Lee, K. Y.; Park, W. H. *J. Biomed. Res., B* **2007**, *83B*, 499−504.
(23) Zhao, R.; Macosko, C. W. *J. Rheol.* **2002**, *46*, 145−167.
(24) Jiang, L.; Lam, Y. C.; Yue, C. Y.; Tam, K. C.; Li, L.; Hu, X. *J. Appl. Polym. Sci.* **2003**, *89*, 1464−1470.
(25) Lam, Y. C.; Jiang, L.; Yue, C. Y.; Tam, K. C.; Li, L. *J. Rheol.* **2003**, *47*, 795−807.
(26) Park, H. E.; Lee, P. C.; Macosko, C. W. *J. Rheol.* **2010**, *54*, 1207−1218.
(27) Robeson, L. M. *Polymer Blends: A Comprehensive Review*; Hanser Gardner: Cincinnati, 2007.
(28) Molau, G. E. *J. Polym. Sci., Part A* **1965**, *3*, 1267−1278.
(29) Wang, D.; Li, Y.; Xie, X. M.; Guo, B. H. *Polymer* **2011**, *52*, 191−200.
(30) Del Castillo-Castro, T.; Castillo-Ortega, M. M.; Herrera-Franco, P. J.; Rodriguez-Felix, D. E. *J. Appl. Polym. Sci.* **2010**, *119*, 2895−2901.
(31) Wei, B.; Genzer, J.; Spontak, R. J. *Langmuir* **2004**, *20*, 8659−8667.
(32) Gozen, A. O.; Zhou, J.; Roskov, K. E.; Shi, A. -C.; Genzer, J.; Spontak, R. J. *Soft Matter* **2011**, *7*, 3268−3272.
(33) Pernot, H.; Baumert, M.; Court, F.; Leibler, L. *Nature Mater.* **2002**, *1*, 54−58.
(34) Yoo, T. W.; Yoon, H. G.; Choi, S. J.; Kim, M. S.; Kim, Y. H.; Kim, W. N. *Macromol. Res.* **2010**, *18*, 583−588.
(35) Godshall, D.; White, C.; Wilkes, G. L. *J. Appl. Polym. Sci.* **2001**, *80*, 130−141.
(36) Lipscomb, G .G. *Polym. Adv. Technol.* **1994**, *5* (11), 745−758.
(37) Arvidson, S. A.; Khan, S. A.; Gorga, R. E. *Macromolecules* **2010**, *43*, 2916−2924.
(38) Mark, J. E., Ed.; *Polymer Data Handbook*; Oxford University Press: New York, 1999.
(39) Sperling, L. H. *Polymeric Multicomponent Materials: An Introduction*; John Wiley & Sons: New York, 1998.
(40) Small, P. A. *J. Appl. Chem.* **1953**, *3*, 71−80.
(41) Hoy, K. L. *J. Paint Technol.* **1970**, *42*, 76−118.
(42) Antonow, G. N. *J. Chim. Phys.* **1907**, *5*, 372−385.
(43) Antonow, G. N. *J. Chim. Phys.* **1907**, *5*, 8.
(44) Biresaw, G.; Carriere, C. J. *J. Polym. Sci. B: Polym. Phys.* **2002**, *40*, 2248−2258.
(45) Helfand, E.; Tagami, Y. *J. Polym. Sci., Part B.* **1971**, *9*, 741−746.
(46) Helfand, E.; Tagami, Y. *J. Chem. Phys.* **1972**, *56* (7), 3592−3601.
(47) Ermoshkin, A. V.; Semenov, A. N. *Macromolecules* **1996**, *29*, 6294−6300.
(48) Gaylord, N. G. *CHEMTECH* **1976**, *6*, 392−395.
(49) Discher, D.; Eisenberg, A. *Science* **2002**, *297*, 967−973.
(50) Lyngaae-Jorgensen, J. K.; Thomsen, D. *Int. Polym. Proc.* **1988**, *3*−*4* (2), 123−130.
(51) Utracki, L. A. *Polymer Alloys and Blends: Thermodynamics and Rheology*; Hanser: Munich, 1989.
(52) Rangasamy, L.; Shim, E.; Pourdeyhimi, B. *J. Appl. Polym. Sci.* **2011**, *121*, 410−419.
(53) Treloar, L. *Trans. Faraday Soc.* **1941**, *37*, 84−97.
(54) Ward, I. *Proc. Phys. Soc.* **1962**, *80*, 1176−1188.
(55) Holden, G., Legge, N. R., Quirk, R. P., Schroeder, H. E., Eds.; *Thermoplastic Elastomers*, 2nd ed.; Hanser: Munich, 1996.
(56) Krishnan, A. S.; Roskov, K. E.; Spontak, R. J. In *Advanced Nanomaterials*; Geckeler, K. E., Nishide, H., Eds.; Wiley-VCH: Weinheim, 2010; pp 791−834.
(57) Krishnan, A. S.; Seifert, S.; Lee, B.; Khan, S. A.; Spontak, R. J. *Soft Matter* **2010**, *6*, 4331−4334.
(58) Kane, L.; Norman, D. A.; White, S. A.; Matsen, M. W.; Satkowski, M. M.; Smith, S. D.; Spontak, R. J. *Macromol. Rapid Commun.* **2001**, *22*, 281−296.
(59) Winey, K. I.; Thomas, E. L.; Fetters, L. J. *J. Chem. Phys.* **1991**, *95*, 9367−9375.
(60) Matsen, M. W. *Macromolecules* **1995**, *28*, 5765−5773.
(61) Raez, J.; Manners, I.; Winnik, M. A. *J. Am. Chem. Soc.* **2002**, *124* (35), 10381−10395.
(62) Wang, X.; Wang, H.; Frankowski, D. J.; Lam, P. G.; Welch, P. M.; Winnik, M. A.; Hartmann, J.; Manners, I.; Spontak, R. J. *Adv. Mater.* **2007**, *19* (17), 2279−2285.
(63) Elbs, H.; Drummer, C.; Abetz, V.; Krausch, G. *Macromolecules* **2002**, *35* (14), 5570−5577.
(64) Dealy, J. M.; Larson, R. G. *Structure and Rheology of Molten Polymers: From Structure to Flow Behavior and Back Again*; Hanser: Munich, 2006.
(65) Laurer, J. H.; Khan, S. A.; Spontak, R. J.; Satkowski, M. M.; Grothaus, J. T.; Smith, S. D.; Lin, J. S. *Langmuir* **1999**, *15* (23), 7947−7955.
(66) O'Connor, K. M.; Pochan, J. M.; Thiyagarajan, P. *Polymer* **1991**, *32* (2), 195−201.
(67) Zhang, W.; Wei, F. Y.; Chen, L.; Zhang, Y. *Proc. 2009 Int. Conf. Adv. Fibers Polym. Mater.*; National Science Foundation of China: Shanghai, 2009; pp 207−209.